# Using terrestrial laser scanner and RPA-based-photogrammetry for surface analysis of a landslide: a comparison

**Article** *in* Boletim de Ciencias Geodesicas · October 2022

DOI: 10.1590/s1982-21702022000300016

CITATIONS
0

READS
106

**4 authors**, including:

Guilherme Pereira Bento Garcia
University of São Paulo
**4** PUBLICATIONS **12** CITATIONS
SEE PROFILE

Carlos Henrique Grohmann
University of São Paulo
**104** PUBLICATIONS **2,094** CITATIONS
SEE PROFILE

Camila Duelis Viana
University of São Paulo
**22** PUBLICATIONS **38** CITATIONS
SEE PROFILE

DOI 10.1590/s1982-21702022000300016

*ORIGINAL ARTICLE*

# Using terrestrial laser scanner and RPA-based-photogrammetry for surface analysis of a landslide: a comparison

Guilherme Pereira Bento Garcia[1] - ORCID: 0000-0003-1209-7842

Carlos Henrique Grohmann[2] - ORCID: 0000-0001-5073-5572

Camila Duelis Viana[3] - ORCID: 0000-0001-7093-0244

Elton Barbosa Gomes[1] - ORCID: 0000-0002-1077-2659

[1]Instituto de Geociências - Universidade de São Paulo, São Paulo - São Paulo, Brasil
E-mails: guilherme.pereira.garcia@usp.br; elton.gomes@alumni.usp.br

[2]Instituto de Energia e Ambiente - Universidade de São Paulo, São Paulo - São Paulo, Brasil
E-mail: camila.viana@usp.br

[3]Prefeitura do Município de São Paulo, Defesa Civil, São Paulo - São Paulo, Brasil
E-mail: guano@usp.br

Received in 06th July 2021.
Accepted in 19th June 2022.

**Abstract:**

Gravitational mass movements are natural destructive processes that can cause enormous losses. New technologies such as laser scanning and remotely piloted aircrafts (RPA) along with photogrammetry technique Structure-from-Motion–Multi-View Stereo (SfM-MVS) photogrammetry technique provides an alternative to conventional mapping methods. A hill with a landslide located in the city of Cunha - SP was surveyed by terrestrial laser scanner (TLS) and RPA-based SfM-MVS. SfM-MVS point cloud covers a larger area and point distribution is more homogeneous while TLS points have an uneven distribution. Small distances between point clouds were predominant in the vicinity of the landslide and greater differences only occurred on the scene edges. DEMs were generated from both point clouds. The volume of material displaced from the upper part (scarp) of the landslide was 70.05 $m^3$ for the TLS DEM and 77.15 $m^3$ for the SfM-MVS while the volume of material accumulated in the lower part (body) of the landslide was 66.85 $m^3$ and 62.68 $m^3$ respectively. Slope and roughness were calculated and showed very similar results for TLS and SfM-MVS.

**Keywords:** LiDAR; SfM-MVS; Landslides; TLS; DEM; Photogrammetry.

**How to cite this article:** Garcia GPB, Carlos Grohmann H, Viana CD, Gomes EB. Using terrestrial laser scanner and RPA-based-photogrammetry for surface analysis of a landslide: a comparison. *Bulletin of Geodetic Sciences*. 28(3): e2022016, 2022.

# 1. Introduction

Hill slopes, mainly unvegetated ones, undergo several erosive processes that can compromise their stability. The occurrence of gravitational mass movements in these slopes is usually triggered by natural phenomena such as rains and earthquakes, which when near to highways or inhabited areas can cause enormous economic losses, environmental harm and life loss (Guerra et al. 2007). Therefore, identification and monitoring of such areas are of high importance.

Landslide mapping methods have changed little throughout the years, with the combination of aerial photography and/or multispectral imagery interpretation, and fieldwork verification still being the standard for the majority of studies (McKean and Roering 2004). A limitation of these 'traditional methods' (Metternicht et al. 2005) is its use in rugged terrain with dense vegetation cover, where the true topography is generally unrecognizable on aerial photographs and multispectral images (van den Eeckhaut et al. 2007). In recent years, more precisely the last two decades, new remote sensing techniques were developed providing more accurate and efficient landslide information.

Both terrestrial (TLS) and airborne (ALS) laser scanning applied to landslides mapping offers many advantages over traditional methods such as fieldwork, topographic map digitization and aerial photography (Booth et al. 2009; Burns and Madin 2009; Shan and Toth 2009; Telling et al. 2017; Vosselman and Maas 2010). It allows generation of high resolution three-dimensional topographic models, being a more accurate method and with little human interference in data acquisition (Rowlands et al. 2003). Rapid data processing with repeated scans and high precision highlights morphometric changes in topography which may indicate sliding process, thus facilitating its identification and monitoring.

The combination of Remotely Piloted Aicrafts (RPAs) and Structure-from-Motion–Multi-view Stereo (SfM-MVS) photogrammetry is becoming an increasingly effective tool to gather outcrop data, particularly in the small- to intermediate-scale range and in areas of difficult access (Chesley et al. 2017).Comparisons between state-of-art lidar data and photogrammetry in landslide studies are recurrent (Carey et al. 2019; Chang et al. 2020; Hung et al. 2019; Mokhtar et al. 2019; Pellicani et al. 2019; Tsunetaka et al. 2020; Yu et al. 2017). Both TLS and RPA-based SfM-MVS have been used for landslide monitoring, mapping and 3D surface reconstruction (Burns et al. 2010; Giordan et al. 2015; Glenn et al. 2006; Godone et al. 2020; Gupta and Shukla 2018; Karantanellis et al. 2019; Rossi et al. 2018; van den Eeckhaut et al. 2011; Xu et al. 2020; Yeh and Chuang 2020). These methods show great advantages over conventional, costly and time consuming ones but also have their own cons which can compromise the entire project.

In this work we compare raw and interpolated point clouds generated by TLS and RPA-based SfM-MVS for the same landslide and evaluate the accuracy of each method by performing a surface analysis. This work is an expansion from Garcia et al. (2019) that only compared the point clouds obtained from TLS and SfM-MVS for the same study area.

## 1.1. Study area

The surveyed area is located in the City of Cunha (São Paulo State, southeastern Brazil), at the roadside of km 40 of the Paulo Virgínio Highway (SP-171), and has approximately 15.000 $m^2$ in area (Fig. 1). The landslide is around 14.5 m long and around 10 m wide, totaling an area of 145 $m^2$. The hillslope has a height amplitude of around 50 m, and is facing S and SW, which makes it more exposed to orographic rainfall from the coast. The area presents sparse vegetation, mainly constituted by tall grass, and soil is partially exposed.

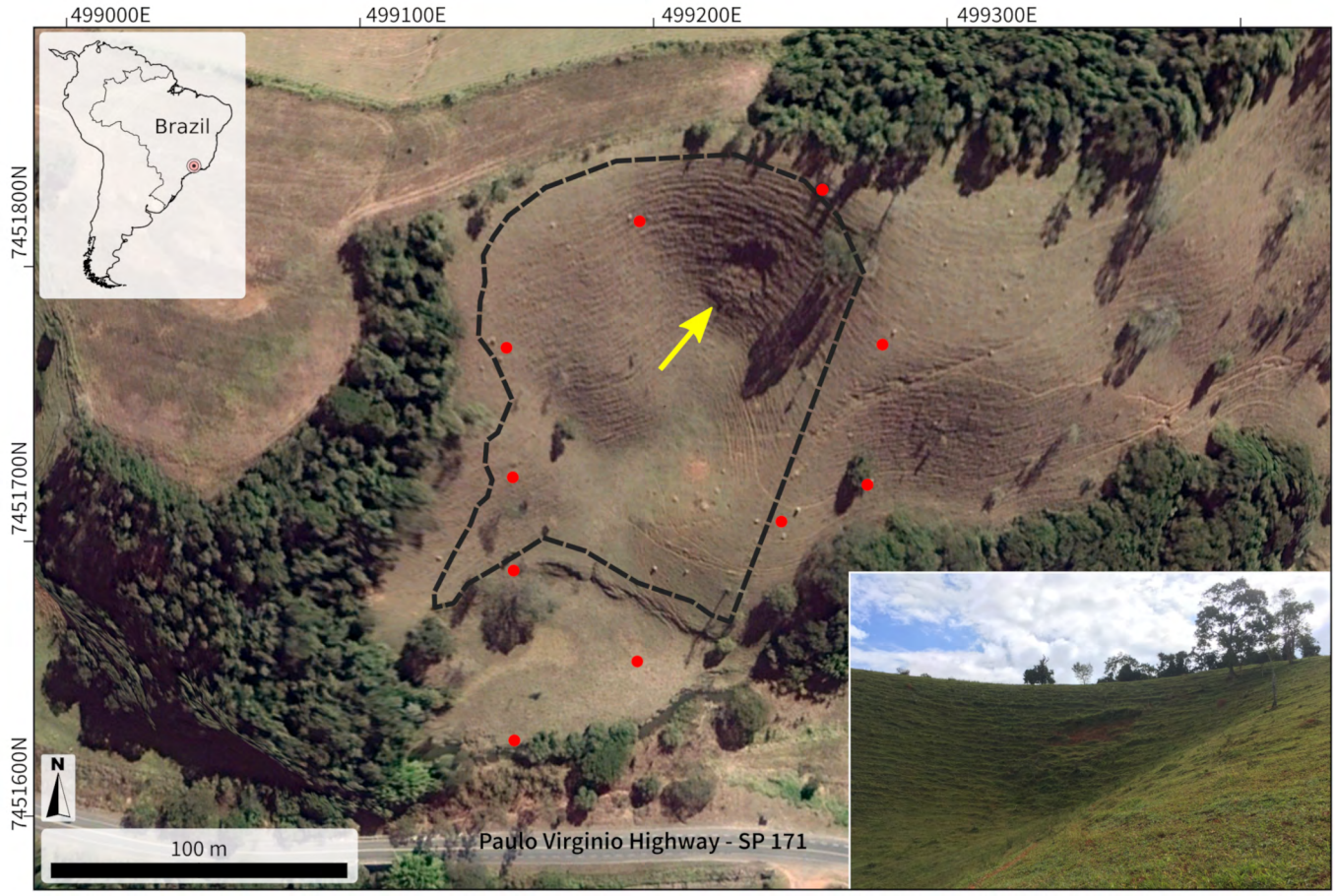


**Figure 1:** Location map of the Cunha City (upper left) and of the study area . Field view of the landslide (right). The dashed line represents the survey boundary,the arrow indicates the area affected by the landslide and the red dots indicates the GCP (Ground Control Points) used for georeferencig. Satellite imagery Digital Globe, powered by Google. UTM coordinates, zone 23 (South), WGS84.

The study area is within the Serra do Mar mountain range, more precisely in the Atlantic Highlands (Planalto Atlantico) Province (Almeida 1964; Ponçano et al. 1981) which is mainly characterized by a rough terrain with high elevation and slopes. The elevations are usually higher than 800 m a.s.l. with local amplitudes up to 300 m, and the slopes are often higher than 20 degrees. These features along with a rainfall pattern higher than 250 mm/month in the wet season, especially in the summer, make this area very susceptible to mass movements, mainly deep-seated and shallow landslides (Perrota et al. 2005).

The municipality of Cunha suffered from several occurrences of mass movements during the summer of 2010-2011, mainly shallow landslides similar to the landslide selected in this study, which was triggered during this period. It was an atypical intense rainfall season that also caused losses in nearby cities within Serra do Mar (Netto et al. 2011).

The geological setting is comprised basically by precambrian basement rocks, mainly metamorphic rocks such as migmatites and gneiss that belongs to the Capivari Complex (Perrota et al. 2005), which occurs as narrow and elongated bands limited by shear zones (Heilbron et al. 2004).

# 2. Methods

## 2.1. Lidar – Terrestrial Laser Scanner

Light Detection and Ranging (lidar) emerge as the main technology and benchmark for landslide studies that uses High-Resolution Digital Elevation Models (HR-DEM) and can be performed in three ways: terrestrial laser scanning (TLS), airborne laser scanning (ALS) and satellite-based laser scanning (Jaboyedoff et al. 2012). Some differences are related to range method, resolution, amount of points gathered and multiple returns (Shan and Toth 2009; Vosselman and Maas 2010).

Terrestrial laser Scanner (TLS) data collection and processing workflows are flexible procedures that are largely controlled by the information desired from the scene being imaged, the physical characteristics of the scene and the surrounding environment (Telling et al. 2017). The selection of the equipment, scan positions, scan registration, georeferencing and point resolution are key elements for the TLS data collection (Shan and Toth 2009; Vosselman and Maas 2010).

The data collection occur with the scanner normally mounted on a tripod and held fixed for the duration of measurements for each position. A single lidar scan collects a large amount of 3D data, several million point measurements, each with x, y and z coordinates and intensity value, which produces a point cloud. To create a point cloud for the entire scene it is necessary to merge all the point clouds from each scan position.

The TLS field survey was performed on May 06, 2018 from 11 stations allocated around the landslide area to generate the TLS point cloud, using a FARO Focus$^S$ 150 LiDAR equipment. The TLS survey took almost all day due to weather conditions and difficult access to positioning/levelling the equipment around the landslide. For georeferencing and point cloud registration, 10 printed targets were evenly distributed around the landslide and surveyed by irradiation using a total station. Coordinates were collected in field by a Spectra Precision 60 (SP60) geodetic GNSS. Post-processing in SPoffice software was used to obtain precise coordinates..

## 2.2. RPA-Based SFM-MVS

SfM-MVS is a workflow employing multiple algorithms developed from 3D computer vision, traditional photogrammetry and conventional survey techniques (Carrivick et al. 2016).

The typical workflow is composed by several steps, each one with specific processing procedures and algorithms, from the detection of image features or keypoints in the photographs to the application of MVS algorithms and point cloud generation (Carrivick et al. 2016). These are standard procedures for 3D scene reconstruction from image sets and are adopted for all SfM-MVS approaches.

The image acquisition was made using a DJI Phantom 4 Pro RPA. The onboard digital camera has an 1” CMOS 20MP sensor, with FOV of 84˚ and 8.8 mm focal distance (24 mm at 35 mm equivalent). The RPA autonomous mission was programmed with the MapPilot App (Drones Made Easy 2017) which allows the flight height to be set as a constant value above a reference DEM (SRTM), resulting in more consistent pixel size values across the imaged area, even in situations of high relief displacement.Two missions were flown on May 06, 2018 to cover the entire hillside, both at 40 m above the terrain, with lateral and frontal overlap of 80% between photos and camera positioned at nadir. For georeferencing and point cloud registration, the same targets and coordinates used for the TLS point cloud were applied. No check points were used in the SfM-MVS process. Each mission lasted around 20 min, the entire RPA survey took about 1 hour.

In this work, we used Agisoft Photoscan Professional version 1.4.5 (Agisoft 2018) software for the 3D reconstruction. The SfM-MVS reconstruction process was set to align images with 'High' accuracy, camera optimization with 0.005 m marker accuracy, 'High' quality and 'aggressive' depth filtering.

The use of the RPA SfM-MVS high resolution data for topographic studies in Brazil is an alternative to expensive and poorly available lidar data. As the landscapes susceptible to landslides in Brazil are predominantly covered by vegetation such as grass and bushes, it is worthwhile to evaluate the potential uses of RPA data compared to state-of-art lidar data in such terrain conditions.

## 2.3. Geomorphometry

For the morphological analysis, both TLS and SfM-MVS point clouds were used to generate DEMs and terrain derivatives. The TLS point cloud was filtered to remove above-surface points that do not represent the terrain, such as tree trunks and termite mounds. The Cloth Simulation Filter (CSF) (Zhang et al. 2016) from CloudCompare software was used to remove points 50 cm above the surface.

Both point clouds were imported in GRASS GIS (GRASS Development Team 2019; Neteler et al. 2012) with the r.in.lidar module, which imports lidar data in LAS format and creates a raster based on univariate statistics of the data. Intermediate rasters were created from the minimum value of LiDAR points within 10 cm cells. These rasters were then interpolated using bilinear splines (r.resamp.bspline – (Brovelli et al. 2004), to fill any void areas and to produce DEMs with spatial resolutions of 10 cm, 50 cm, 1 m and 2 m, which were used to evaluate the capacity of each surface in resolving fine to medium scale landslide features.

The landslide analysis is comprised by a morphometric analysis and an estimation of the volume of displaced material. Morphometric parameters commonly used in landslide analysis were computed, namely slope and surface roughness (Glenn et al. 2006; Grohmann et al. 2011; McKean and Roering 2004), and used for comparison of TLS and SfM-MVS results.

The volume estimation can be performed by subtracting DEMs created before and after the landslide event. The 'before' DEM is usually generated by the interpolation of topographic maps prior the landslide (Du and Teng 2007); however, there are no high-resolution topographic data available for the study area before 2011 to enable the creation of a DEM representing the terrain before the landslide.

Thus, the surface was manually reconstructed based on a contour map with 50 cm interval derived from the current 10 cm spatial resolution DEM: the contour lines deformed by the landslide were reconstructed following the intact contour lines from surrounding areas (Fig. 2). This reconstructed contour map was interpolated with bilinear splines to generate a new DEM with 50 cm spatial resolution, representing the surface before the landslide. The manual reconstruction of the surface was performed only for the 10 cm TLS interpolated DEM and the reconstructed surface DEM was used as the reference data for the volume estimation.

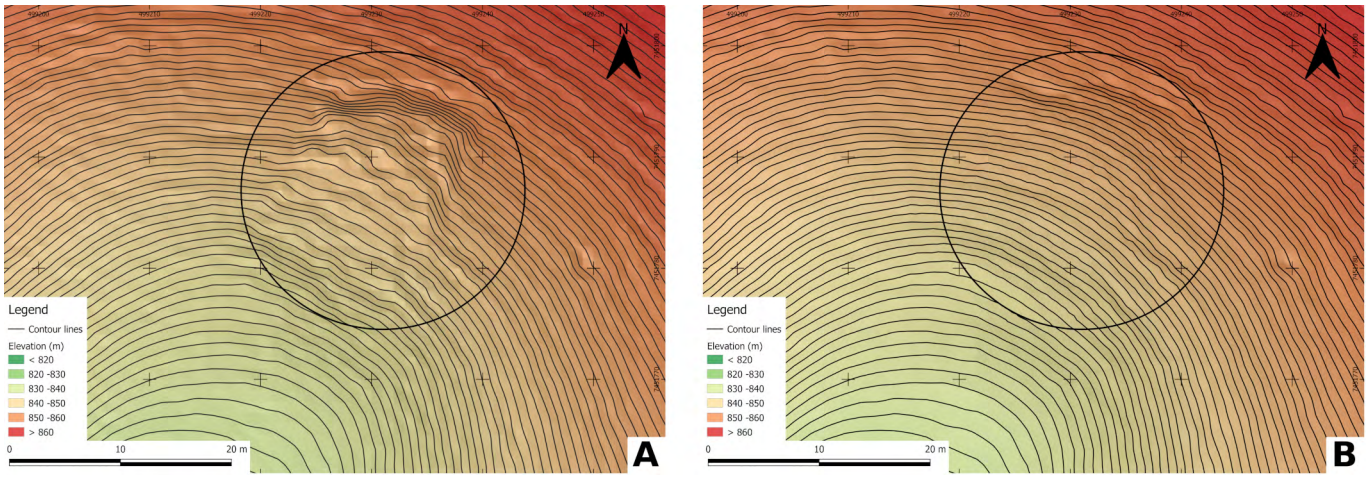


**Figure 2:** Reconstruction of topography for volume calculation. A) Contour lines deformed by the slide event; B) Contour lines reconstruction. Example from the TLS point cloud DEM with 50 cm spatial resolution and contour lines with 50 cm interval.

Surface roughness measures the variability of the topographic surface at a given scale (e.g., Berti et al. 2013; Grohmann et al. 2011) and it has been widely used in landslide studies. There are several algorithms to compute surface roughness with the Terrain Ruggdness Index (TRI) (Riley et al. 1999) and the standard deviation of elevation (Glenn et al. 2006; McKean and Roering 2004) being the most popular. Grohmann et al. (2011) computed and compared different surface roughness algorithms in various scales and with different sizes of moving windows; the standard deviation of slope was the most accurate surface roughness algorithm in detecting fine scale/regional relief and showed the best performance at a variety of scales.

In this study, surface roughness was calculated as the standard deviation of slope for both TLS and SfM-MVS DEMs with four different spatial resolutions (10 cm, 50 cm, 1 m and 2 m) with a 3x3 window size. This combination was meant to determine which scale is more accurate for the landslide analysis.

The generation of DEMs, contour maps and terrain derivatives were all performed using the Free and Open Source Software QGIS (QGIS Development Team 2019) grass and

# 3. Results and discussion

## 3.1. Point cloud comparison

FARO SCENE was used for processing the raw TLS data and create a single point cloud from the individual scans. All markers were automatically recognized by FARO SCENE. The resulting TLS point cloud has 128,513,743 points (Fig. 3A).

The TLS point cloud, despite having a larger number of points, does not represent the entire area equally. The point distribution is denser near the scans positions, gradually decreasing with distance. Voids are common, mainly further from the slide area where less information was captured. Even the landslide area has some occlusions which would require more scans from different viewpoints to fill them.

The SfM-MVS point cloud (Fig. 3B) was generated with Agisoft Photoscan (Agisoft 2018) using 315 images. The complete SfM-MVS workflow, using the 'high quality' settings of Photoscan, produced a dense cloud with

93,245,315 points. Only 7 markers were identified in the image set, as the vertical position of some markers – specially one at a tree trunk that was covered by its crown on the images – makes it difficult to locate them in the vertical RPA images.

The SfM-MVS point cloud has a more uniform appearance, as points are homogeneously distributed and there are no significant voids. The slope is entirely comprised within the point cloud and the landslide can be clearly identified. This point cloud has approximately 35 million points less than the TLS point cloud but covers a larger area.

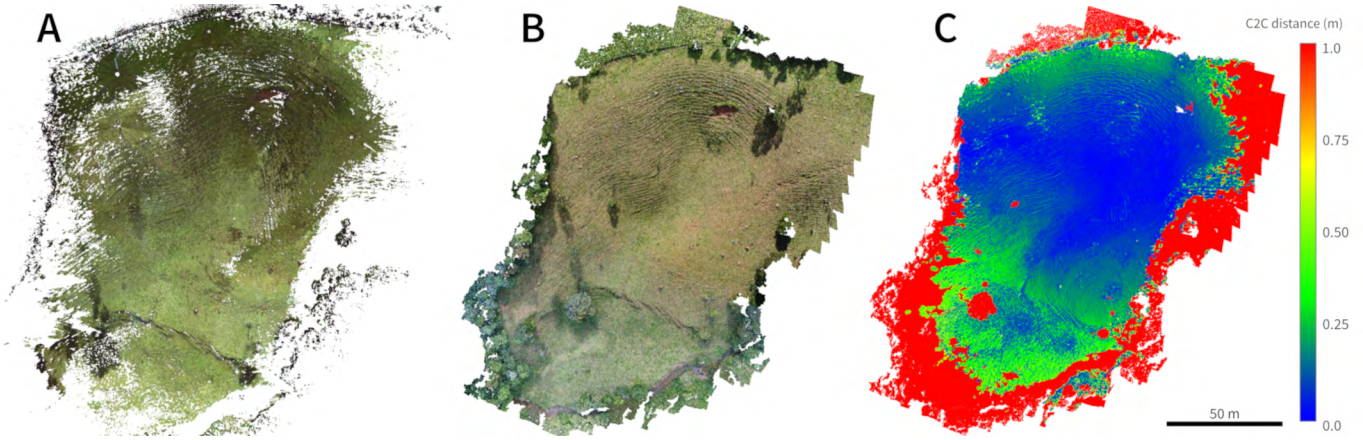


**Figure 3:** A) TLS point cloud; B) SfM-MVS point cloud; C) Cloud-to-Cloud distance with 1 m threshold using the TLS as the reference cloud.

The difference between the two clouds was computed using the "Cloud-to-Cloud distance" tool in CloudCompare (Fig. 3C). Distances less than 50 cm are predominant in the entire area overlapped by the point clouds with distances less than 15 cm comprising the landslide area. The TLS did not acquired points far from the scan positions, concentrating them within the slope, while the RPA captured a wider area and the SfM-MVS method generated a homogeneous point cloud. Larger distances (>1 m) between the point clouds occur at the borders of the surveyed area, probably beyond TLS scan range or due the presence of ground obstacles blocking the laser beam path. However, points within the slope are very similar even though the TLS point cloud being denser than the SfM-MVS one.

Small differences could be related to georeferencing, since the RPA images do not capture vertical targets precisely, like the TLS does from a ground position. Fig.4 shows an example of how the RPA imaged a vertical marker. This marker was placed over a termite mound and was in a near vertical position, hindering the correct determination of its center Some markers were not visible in the RPA images, affecting the distribution of ground control information and thus affecting georeferencing.

Absence of vegetation also contributes to this smalls differences. RPA images are in visible spectral range (RGB) so it has no penetration through leaves. Densely vegetated areas hide markers in the RPA images, which increases georeferencing errors and point cloud differences.

Both TLS and SfM-MVS point clouds are suitable for 3D surface modelling in this case. Point clouds differences are minimal in the target area, despite the 35 million points variation between them. Larger differences occur only outside the study area and have less influence in the final models. Absence of vegetation allows generation of digital models from both point clouds without significant information loss.


**Figure 4:** RPA image of a printed target, placed in a near-vertical position over a termite mound.

## 3.2. Morphological analysis

The landslide was divided in two parts for the volume estimation computation: 1- the upper part (scarp of the landslide) from where the material was removed and has the soil exposed; and, 2- the lower part (body of the landslide) where the material accumulated and its covered by grass and some bushes. The volume was estimated for each part separately and for both TLS and RPA SfM-MVS 10 cm DEMs using the 10 cm TLS DEM with the surface reconstructed as the reference.

Prior the volume calculation it was expected some differences in the results from the upper and lower part of the landslide due to erosion process or the swell factor that happened over the years since the landslide occurrence in 2011 (Dewitte and Demoulin 2005; Pedrazzini et al. 2010; Schulz et al. 2018).

The volume estimation from the TLS DEM with 10 cm resolution showed that 70.05 $m^3$ of material was displaced from the upper part and 66.85 $m^3$ of material accumulated in the lower part. For the SfM-MVS DEM with 10 cm spatial resolution the volume estimation was 77.15 $m^3$ of material displaced from the upper part and 62.68 $m^3$ of material accumulated in the lower part.

The differences between the TLS and RPA SfM-MVS volumes estimation for the upper (TLS: 70.05 $m^3$; RPA: 77.15 $m^3$; $\Delta$ = 7.10 $m^3$) and lower part (TLS: 66.85 m3; RPA: 62.68 $m^3$; $\Delta$ = 4.17 $m^3$) was probably related to points density, RPA camera position in the image acquisition process and the presence of vegetation.

The main volume differences occur in the upper part ($\Delta$ = 7.10 $m^3$) and must be related to point density or RPA camera position. Point cloud comparison in section 3.1 showed that even though the TLS point cloud has around 35 millions points more than the SfM-MVS point cloud, the TLS point distribution is denser near the scans positions, and it presented occlusions in the landslide area, which may affect the interpolation process and contribute to volume difference in the upper part. However, the nearly vertical position of the landslide scarp makes the RPA image acquisition process difficult with the camera in the nadir position because it does not have a clear view of the whole scarp. The interpolation process for the SfM-MVS point cloud probably smooths the surface if the scarp which creates differences from the TLS DEM. Figure 5 shows three profiles in the upper part of the landslide comparing TLS and SfM-MVS DEMs.

The volume difference in the lower part ($\Delta$ = 4.15 $m^3$) is more feasible and is probably related to the presence of undergrowth or minor errors caused by the georeferencig process discussed in section 3.1. The lower part is covered

with vegetation, mainly tall grass with dozens of centimeters, that prevented the RPA from obtaining bare earth points and was filtered in the TLS point cloud but remain intact in the SfM-MVS data. This grass made it impossible to reconstruct the topography and create a DTM from the RPA SfM-MVS point cloud, a DSM was generated instead which is not accurate as lidar-derived DTM in vegetated areas (Niethammer et al. 2010; Yu et al. 2017).

Although the comparison between the TLS DTM and the SfM-MVS DSM is not ideal, it allows to evaluate major differences between them and whether they have any degree of similarities in morphological analysis.

Also it was possible to estimate the weight of the displaced material. The study area is comprised with red-yellow oxisol which its density vary from 1.0 to 1.4 g/cm³ (Ferreira et al. 2015; Spera et al. 2002; Torres and Saraiva 1999). For the weight calculation an average density of 1.2 g/cm³ was considered. The landslide dimensions were 14.5 m long and 10 m wide with a total area of 145 m². The volume of material displaced from the upper part was estimated in 70.05 m³ from the TLS data and the scarp has 2 m height. The estimation weight of the displaced material was about 84 tons.

The study area has great slope variability with the values at the N and W portions usually higher than 35 degrees and the S and E portions up to 20 - 25 degrees. The landslide occurred in the NE portion of the catchment area which corresponds to the highest slope values, above 45 degrees.

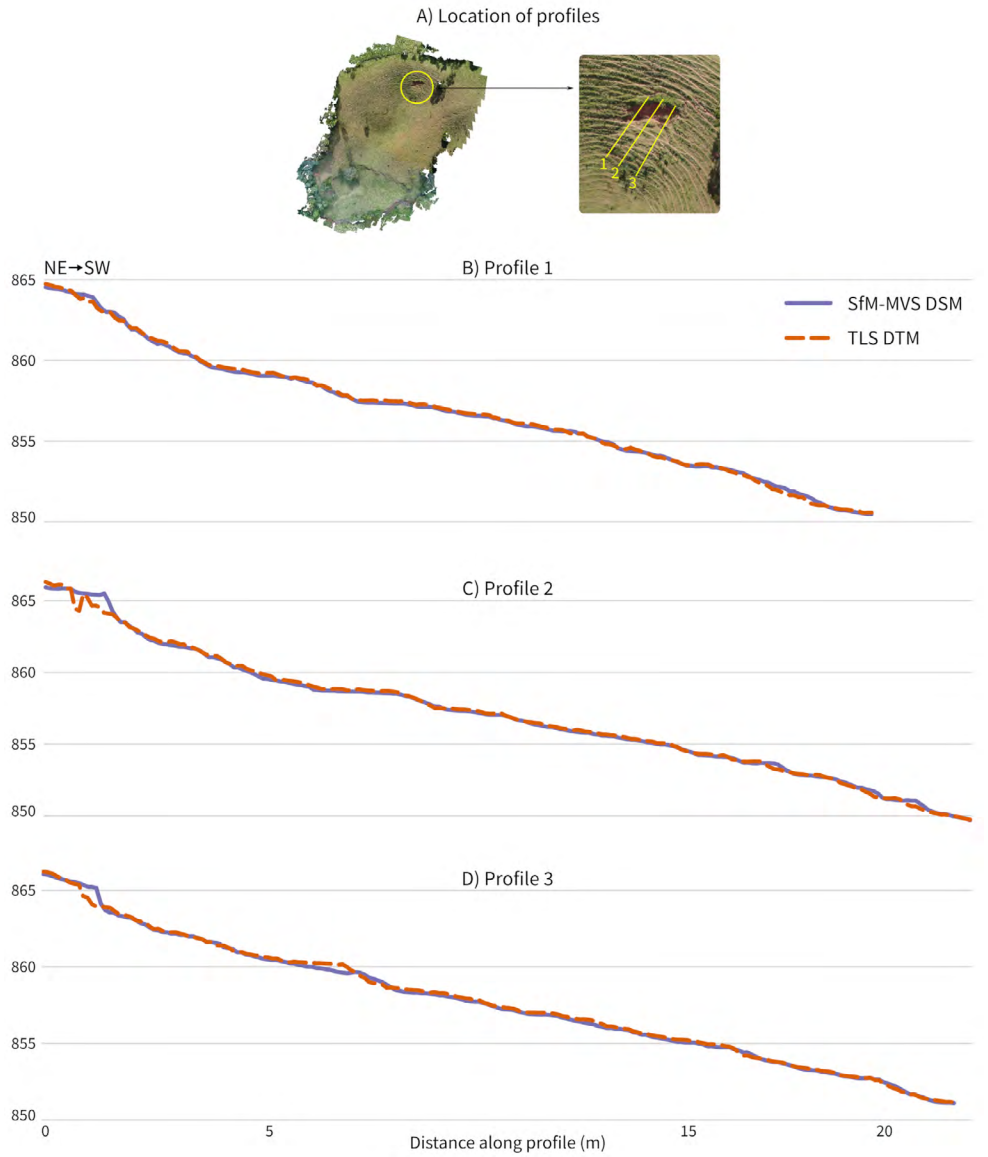


**Figure 5:** Landslide profiles comparing TLS and SfM-MVS point clouds.

The slope maps with spatial resolutions of 50 cm are the more accurate in delineating the landslide, both scarp and body were detected (Figs. 6B,6F). The 10 cm resolution slope maps enhance non-terrain features such as termite mounds and tree trunks that are common in the study area and the visual interpretation is impaired by the salt-and-pepper effect (Figs. 6A,6E). The maps with 1 m and 2 m spatial resolution (Figs. 6C,D,G,H) are more widespread but are also able to correctly detect the landslide, mainly the scarp that is clearly distinguishable from the surroundings. The non-terrain features are more clearly observed in the SfM-MVS slope maps, probably because the SfM-MVS point cloud could not be filtered before the DEM generation.

Both TLS and SfM-MVS DEMs showed very similar slope results from all the spatial resolutions used. This high similarity was expected once both TLS and SfM-MVS point clouds had minimal differences in the landslide area.

The surface roughness maps (Figs. 6I-P) were classified in five categories: very low (flat terrain), low, medium, high and very high (rugged terrain). The roughness categories were defined from the histogram of each spatial resolution DEM, thus TLS and SfM-MVS DEM with the same spatial resolution had the same classification once the histograms were very similar with near maximum values. The histogram shows how many standard deviations occur at each pixel, the higher the standard deviation the rougher is the terrain. The scarp of the landslide is the most prominent portion detected, the body and toe of the landslide cannot be clearly distinguished due the small size of the landslide but the area beneath the landslide is much smoother than the adjacent areas.

The highest values of surface roughness occur in the landslide scarp and surrounding areas which indicates that these areas were already rougher before the landslide. The predominant rugged parts of the hillslope are probably related to cattle passage, that forms step-like features, which are easily recognized in the fine scale surface roughness maps, mainly in the 10 cm spatial resolution with 3x3 window (Figs. 6I,M). These cattle passage features enhance landslide susceptibility in the hillslope by preventing vegetation growth and exposing the soil, which contributes to erosion process (Fiori and Carmignani 2015).

The surface roughness maps derived from TLS and SfM-MVS DEMs showed some similarities to each other in all combinations of spatial resolution except in the 1 m spatial resolution DEM where there are huge differences between TLS and SfM-MVS maps (Figs. 6K,O). Overall, TLS roughness maps are more accurate in delineating the landslide than SfM-MVS results, with cleaner and more homogeneous images.

For the study area, the fine scale maps (10 cm and 50 cm) are very detailed and comprised features such as termite mounds, which are not part of the terrain and can lead to misinterpretations. The 50 cm spatial resolution roughness maps from both TLS and SfM-MVS (Figs. 6J,N) are the best in detecting the scarp of the landslide with less distortion caused by other terrain features, but did not detected the body of the landslide clearly and the SfM-MVS map had more disturbance from adjacent areas.

Roughness maps with coarser spatial resolutions (1 m and 2 m) are very affected by terrain features other than the landslide parts and had a more erroneous classification. The landslide area can be detected with these maps, mainly in the 1 m TLS map, but it is not possible to determine the boundaries of the landslide parts with certainty which leads to misinterpretation. The 2 m spatial resolution maps presents some pattern of the rougher parts that are clearly connected to the landslide and may indicate preferred paths of the erosion processes. The maps with 1 m spatial resolution are very different while TLS map classification is in accordance with the other maps detecting the rougher parts in a similar way, the SfM-MVS map is highly heterogeneous and chaotic with no patterns and similarities to others roughness map.

# 4. Conclusions

A hill slope with a minor landslide (14.5 m long and 10 m wide), mainly covered by grass and with partially exposed soil was scanned by a TLS and photographed by an RPA, generating two point clouds. Vegetation absence

is critical for comparing both methods since the RPA images cannot register information below the canopy. The final TLS point cloud contains 128,513,743 points while RPA , generated by SfM-MVS, 93,245,315 points, a difference of about 35 million points. The two point clouds were very similar in the top and center slope areas but presented large differences at the borders of the scene.

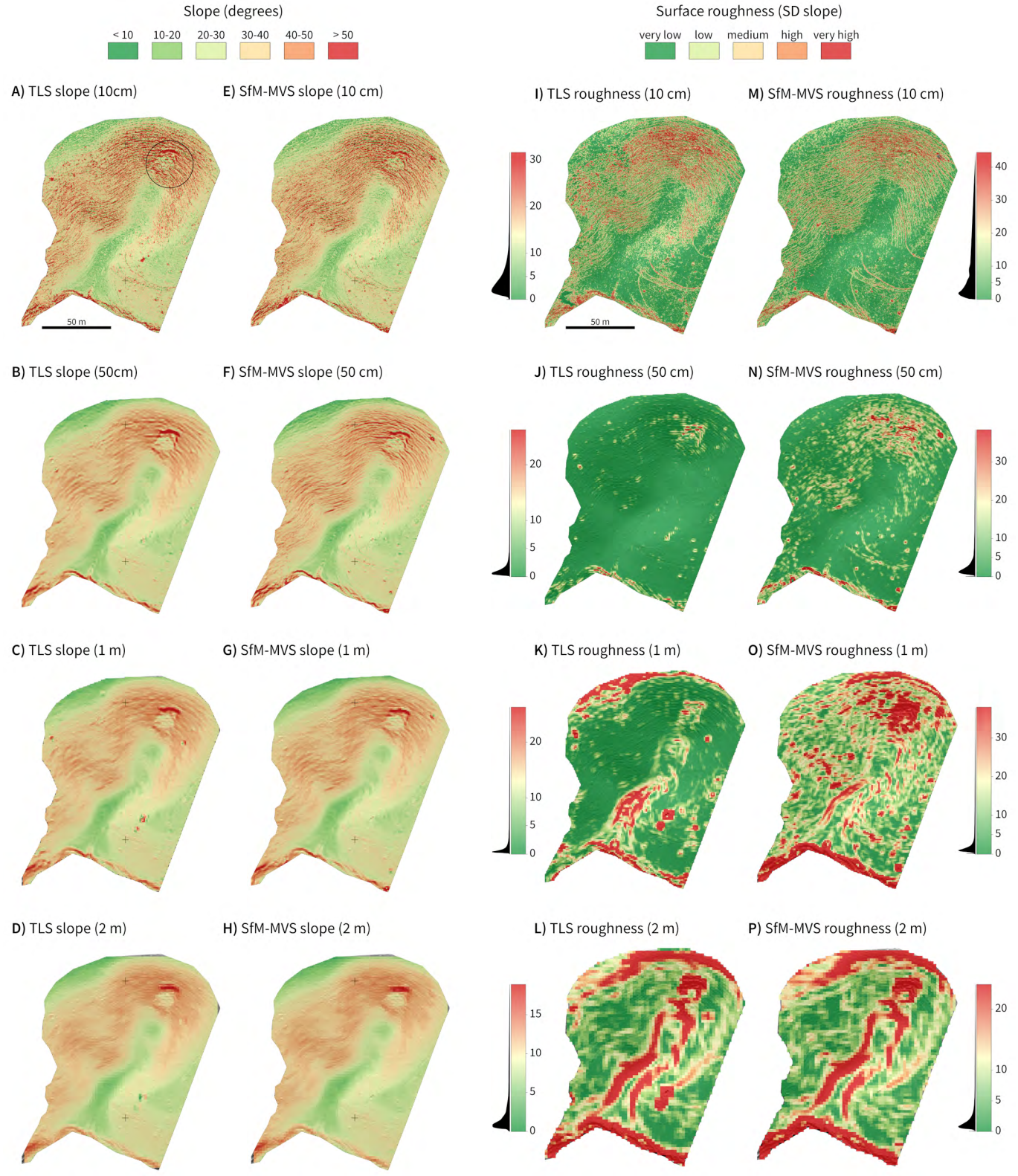


**Figure 6:** A-D) TLS slope; E-H) SfM-MVS slope; I-L) TLS surface roughness; M-P) SfM-MVS surface roughness.

TLS technical limitations (such as laser beam path obstruction) can explain the major differences in the borders of the scene, while georeferencing problems probably causes small differences within the slope. The RPA images were taken at nadir angle, so ground control points markers in a near-vertical position (such as in tree trunks or termite mounds) are not precisely identified, and this can lead to these minor errors in the point clouds.

The TLS DEM estimation of material displaced from the upper part was of 70.05 $m^3$ and the estimation of material accumulated in the lower part was 66.85 $m^3$, while the SfM-MVS DEM estimation for material displacement and accumulation was 77.15 $m^3$ and 62.68 $m^3$ respectively. The differences in the volume estimation results between TLS and RPA SfM-MVS DEMs can be addressed to point density, RPA camera position and presence of vegetation, instead of accuracy of the methods.

Both TLS and SfM-MVS slope maps accurately identified the landslide in all the spatial resolutions and classified the whole area in a similar way. Some differences occurred in the min-max slope values but this must be related to georeferencing problems and points acquisition process. The SfM-MVS point cloud was not filtered like the TLS point cloud, so points off the terrain such as tree trunks and termite mounds must be present in the DEM and influenced the slope calculation.

TLS and SfM-MVS roughness maps had similarities but presented important differences. In both cases 50 cm spatial resolution maps were the more accurate correctly delineating the landslide area from surroundings. Fine scale maps (10 cm and 50 cm) enhances features not related to the terrain and enables visualization of cattle passage features that contributes to the increase of surface erosion processes which leads to greater landslide susceptibility.

For this specific terrain conditions, with no vegetation cover and few view obstacles, both point clouds are suitable for DEM generation and other surface modelling to identify landslides. The concentration of TLS points in the landslide area should provide more detailed DEMs than SfM-MVS, but for local and intermediate scales both methods can be applied with minimal information loss.

The choice of which method is a better fit a project will be determined by budget, mapping scale and characteristics of the study area. Other studies comparing TLS, ALS and SfM-MVS in different environments should provide distinct results. Potential advantages of RPA-based SfM-MVS include smaller cost both in terms of equipment and processing time, although its efficacy is limited by the presence of vegetation.

## ACKNOWLEDGMENT

This study was supported by the Sao Paulo Research Foundation (FAPESP) grants #2016/06628-0, #2019/26568-0 and by Brazil's National Council of Scientific and Technological Development, CNPq grants #311209/2021-1, #423481/2018-5, #304413/2018-6 to C.H.G. This study was financed in part by CAPES Brasil - Finance Code 001 through a PhD scholarship to G.P.B.G. This work acknowledges the services provided by the OpenTopography Facility with support from the National Science Foundation under NSF Award Numbers 1557484, 1557319, and 1557330. Acknowledgments are extended to the Editor-in-Chief, the Associate Editor, and the anonymous reviewers for their criticism and suggestions, which helped to improve this paper.

## AUTHOR´S CONTRIBUTION

Conceptualization, G.P.B.G, C.H.G., C.D.V., E.G.; methodology, C.H.G., G.P.B.G, C.D.V.; formal analysis, G.P.B.G, C.D.V., E.G; writing--original draft preparation, G.P.B.G, C.H.G.; writing--review and editing, G.P.B.G, C.H.G., C.D.V.; visualization, C.H.G., G.P.B.G, E.G.; supervision, C.H.G.; project administration, C.H.G.; funding acquisition, C.H.G.

# REFERENCES

Agisoft. (2018). AgiSoft Photoscan Professional Software.

Almeida, F. F. M. (1964). Fundamentos geológicos do relevo paulista. *Boletim do IGG*, *41*, 169–263.

Berti, M., Corsini, A., & Daehne, A. (2013). Comparative analysis of surface roughness algorithms for the identification of active landslides. *Geomorphology*, *182*, 1–18. https://doi.org/10.1016/j.geomorph.2012.10.022

Booth, A. M., Roering, J. J., & Perron, J. T. (2009). Automated landslide mapping using spectral analysis and high-resolution topographic data: Puget Sound lowlands, Washington, and Portland Hills, Oregon. *Geomorphology*, *109*(3–4), 132–147. https://doi.org/10.1016/j.geomorph.2009.02.027

Brovelli, M. A., Cannata, M., & Longoni, U. M. (2004). LIDAR Data Filtering and DTM Interpolation Within GRASS. *Transactions in GIS*, *8*(2), 155–174. https://doi.org/10.1111/j.1467-9671.2004.00173.x

Burns, W. J., Coe, J. A., Kaya, B. S., & Ma, L. (2010). Analysis of elevation changes detected from multi-temporal LiDAR surveys in forested landslide terrain in western Oregon. *Environmental and Engineering Geoscience*, *16*(4), 315–341. https://doi.org/10.2113/gseegeosci.16.4.315

Burns, W. J., & Madin, I. P. (2009). *Protocol for Inventory Mapping of Landslide Deposits from Light Detection and Ranging (lidar) Imagery* (No. 42). Portland, OR.

Carey, J. A., Pinter, N., Pickering, A. J., Prentice, C. S., & Delong, S. B. (2019). Analysis of landslide kinematics using multi-temporal unmanned aerial vehicle imagery, La Honda, California. *Environmental & Engineering Geoscience*, *25*(4), 301–317.

Carrivick, J. L., Smith, M. W., & Quincey, D. J. (2016). *Structure from motion in the geosciences* (1st ed.). Oxford, UK: John Wiley & Sons, Ltd.

Chang, K.-J., Tseng, C.-W., Tseng, C.-M., Liao, T.-C., & Yang, C.-J. (2020). Application of Unmanned Aerial Vehicle (UAV)-Acquired Topography for Quantifying Typhoon-Driven Landslide Volume and Its Potential Topographic Impact on Rivers in Mountainous Catchments. *Applied Sciences*, *10*(17), 1–16. https://doi.org/10.3390/app10176102

Chesley, J. T., Leier, A. L., White, S., & Torres, R. (2017). Using unmanned aerial vehicles and structure-from-motion photogrammetry to characterize sedimentary outcrops: An example from the Morrison Formation, Utah, USA. *Sedimentary Geology*, *354*, 1–8. https://doi.org/10.1016/j.sedgeo.2017.03.013

Dewitte, O., & Demoulin, A. (2005). Morphometry and kinematics of landslides inferred from precise DTMs in West Belgium. *Natural Hazards and Earth System Sciences*, *5*(2), 259–265. https://doi.org/10.5194/nhess-5-259-2005

Drones Made Easy. (2017). MapPilot . San Diego, CA.

Du, J. C., & Teng, H. C. (2007). 3D laser scanning and GPS technology for landslide earthwork volume estimation. *Automation in Construction*, *16*(5), 657–663. https://doi.org/10.1016/j.autcon.2006.11.002

Ferreira, R. M. F., Ferreira, V. M., Filho, J. T., & Ralisch, R. (2015). Qualidade Físico-Hídrica De Cambissolo Sob Pastagem Extensiva. In *XXI Simposio Brasileiro de Recursos Hidricos* (pp. 1–8). Brasilia, DF.

Fiori, A. P., & Carmignani, L. (2015). *Fundamentos de mecânica dos solos e das rochas: aplicações na estabilidade de taludes*. (A. P. Chaves, C. G. Silva, D. C. C. K. Kowaltowski, J. G. Tundisi, L. E. Sánchez, P. Helene, et al., Eds.) (3rd ed.). São Paulo: Oficina dos Textos.

Garcia, G. P. B., Gomes, E. B., Viana, C. D., & Grohmann, C. H. (2019). Comparing Terrestrial Laser Scanner and UAV-based Photogrammetry to Generate a Landslide DEM . In *Anais do XIX Simpósio Brasileiro de Sensoriamento Remoto* (pp. 415–418). Santos: INPE.

Giordan, D., Manconi, A., Tannant, D. D., & Allasia, P. (2015). UAV: low-cost remote sensing for hig-resolution investigation of landslides. In *IEEE International Geoscience and Remote Sensing Symposium* (pp. 5344–5347).

Glenn, N. F., Streutker, D. R., Chadwick, D. J., Thackray, G. D., & Dorsch, S. J. (2006). Analysis of LiDAR-derived topographic information for characterizing and differentiating landslide morphology and activity. *Geomorphology*, *73*(1–2), 131–148. https://doi.org/10.1016/j.geomorph.2005.07.006

Godone, D., Allasia, P., Borrelli, L., & Gulla, G. (2020). UAV and structure from motion approach to monitor the Maierato landslide evolution. *Remote Sensing*, *12*(6), 1039–1057. https://doi.org/https://doi.org/10.3390/rs12061039

GRASS Development Team. (2019). Geographic Resources Analysis Support System (GRASS GIS) Software. Open Source Geospatial Foundation.

Grohmann, C. H., Smith, M. J., & Riccomini, C. (2011). Multiscale Analysis of Topographic Surface Roughness in the Midland Valley, Scotland. *IEEE Transactions on Geoscience and Remote Sensing*, *49*(4), 1200–1213. https://doi.org/10.1109/TGRS.2010.2053546

Guerra, A. J. T., Gonçalves, L. F. H., & Lopes, P. B. M. (2007). Evolução Histórico-Geográfica Da Ocupação Desordenada E Movimentos De Massa No Município De Petrópolis, Nas Últimas Décadas. *Revista Brasileira de Geomorfologia*, *8*(1), 35–43. https://doi.org/10.20502/rbg.v8i1.84

Gupta, S. K., & Shukla, D. P. (2018). Application of drone for landslide mapping, dimension estimation and its 3D reconstruction. *Journal of the Indian Society of Remote Sensing*, *46*(6), 903–914. https://doi.org/https://doi.org/10.1007/s12524-017-0727-1

Heilbron, M., Pedrosa-Soares, A. C., Campos Neto, M. C., Silva, L. C., Trouw, R. A. J., & Janasi, W. A. (2004). Província Mantiqueira. In V. Mantesso-Neto, A. Bartorelli, C. D. R. Carneiro, & B. B. Brito-Neves (Eds.), *Geologia do Continente Sul-Americano: Evolução da obra de Fernando Flávio Marques de Almeida* (1st ed., pp. 203–236). São Paulo, Brasil: Beca.

Hung, C. L. J., Tseng, C. W., Huang, M. J., Tseng, C. M., & Chang, K. J. (2019). Multi-temporal high-resolution landslide monitoring based on UAS photogrammetry and UAS lidar geoinformation. In *Geoinformation for Disaster Management* (pp. 157–160). Prague, Czech Republic. https://doi.org/https://doi.org/10.5194/isprs-archives-XLII-3-W8-157-2019

Jaboyedoff, M., Oppikofer, T., Abellán, A., Derron, M. H., Loye, A., Metzger, R., & Pedrazzini, A. (2012). Use of LIDAR in landslide investigations: A review. *Natural Hazards*, *61*(1), 5–28. https://doi.org/10.1007/s11069-010-9634-2

Karantanellis, E., Marinos, V., & Vassilakis, E. (2019). 3D hazard analysis and object-based characterization of landslide motion mechanism using UAV imagery. In *ISPRS Geospatial Week* (pp. 425–430). Enschede, The Netherlands. https://doi.org/https://doi.org/10.5194/isprs-archives-XLII-2-W13-425-2019

McKean, J., & Roering, J. (2004). Objective landslide detection and surface morphology mapping using high-resolution airborne laser altimetry. *Geomorphology*, *57*(3–4), 331–351. https://doi.org/10.1016/S0169-555X(03)00164-8

Metternicht, G., Hurni, L., & Gogu, R. (2005). Remote sensing of landslides: An analysis of the potential contribution to geo-spatial systems for hazard assessment in mountainous environments. *Remote Sensing of Environment*, *98*(2–3), 284–303. https://doi.org/10.1016/j.rse.2005.08.004

Mokhtar, N. M., Darwin, N., Ariff, M. F. M., Majid, Z., & Idris, K. M. (2019). The capabilities of unmanned aerial vehicle for slope classification. In *6th International Conference on Geomatics and Geospatial Technology* (pp. 451–459). Kuala Lumpur, Malaysia. https://doi.org/https://doi.org/10.5194/isprs-archives-XLII-4-W16-451-2019

Neteler, M., Bowman, M. H., Landa, M., & Metz, M. (2012). GRASS GIS: A multi-purpose open source GIS. *Environmental Modelling & Software*, *31*, 124–130. https://doi.org/10.1016/j.envsoft.2011.11.014

Netto, A. L. C., Sato, A. M., Avelar, A. S., Vianna, L. G. G., Araújo, I. S., Ferreira, D. L. C., et al. (2011). January 2011: the extreme landslide disaster in Brazil. In *Proceedings of the 2nd Worl landslide Forum* (p. 6). https://doi.org/10.1007/978-3-642-31319-6_51

Niethammer, U., Rothmund, S., James, M. R., Travelletti, J., & Joswig, M. (2010). UAV-Based Remote Sensing of Landslides. In *International Archives of Photogrammetry, Remote Sensing and Spatial Information Sciences* (pp. 496–501).

Pedrazzini, A., Abellán, A., Oppikofer, T., Ambrosi, C., Spataro, A., & Jaboyedoff, M. (2010). Retrogressive landslide monitoring by TLS: precursory displacements and final collapse. Case study at Val Canaria (Ticino, Switzerland). *Geophysical Research Abstracts, EGU General Assembly 2010*, *12*. http://meetingorganizer.copernicus.org/EGU2010/EGU2010-12160.pdf

Pellicani, R., Argentiero, I., Manzari, P., Spilotro, G., Mazzo, C., Ermini, R., & Apollonio, C. (2019). UAV and airborne lidar data for interpreting kinematic evolution of landslide movements: the case study of the Montescaglioso landslide (Southern Italy). *Geosciences*, *9*(6), 1–18. https://doi.org/https://doi.org/10.3390/geosciences9060248

Perrota, M. M., Salvador, E. D., Lopes, R. C., D'Agostino, L. Z., Peruffo, N., Gomes, S. D., et al. (2005). *Mapa Geológico do Estado de São Paulo*. São Paulo, Brasil.

Ponçano, V., Carneiro, C., Bistrichi, C., Almeida, F., & Prandini, F. (1981). *Mapa geomorfológico do Estado de São Paulo, escala 1:1.000.000* (1183rd ed., Vol. 2). São Paulo: IPT.

QGIS Development Team. (2019). QGIS Geographic Information System . Open source Geospatial Foundation.

Riley, S. J., DeGloria, S. D., & Elliot, R. (1999). A terrain ruggedness index that quantifies topographic heterogeneity. *Journal of Soil Science* , *5*, 23–27.

Rossi, G., Tanteri, L., Tofani, V., Vannocci, P., Moretti, S., & Casagli, N. (2018). Multitemporal UAV surveys for landslide mapping and characterization. *Landslides*, *15*, 1045–1052. https://doi.org/DOI 10.1007/s10346-018-0978-0

Rowlands, K. A., Jones, L. D., & Whitworth, M. (2003). Landslide laser scanning: a new look at an old problem. *Quarterly Journal of Engineering Geology and Hydrogeology*, *36*(2), 155–157.

Schulz, W. H., Smith, J. B., Wang, G., Jiang, Y., & Roering, J. J. (2018). Clayey Landslide Initiation and Acceleration Strongly Modulated by Soil Swelling. *Geophysical Research Letters*, *45*(4), 1888–1896. https://doi.org/10.1002/2017GL076807

Shan, J., & Toth, C. K. (2009). *Topographic Laser Ranging and Scanning: Principles and Processing*. (J. Shan & C. K. Toth, Eds.) (1st ed.). Boca Raton, FL: Taylor & Francis Group LLC.

Spera, S. T., Reatto, A., Martins, É. de S., Farias, M. F. R., Silva, Â. V., Júnior, O. A. de C., & Guimarães, R. F. (2002). *Solos e Aptidão Agricola das Terras da Área de Proteção Ambiental de cafuringa, Distrito federal*. Planaltina, DF.

Telling, J., Lyda, A., Hartzell, P., & Glennie, C. (2017). Review of Earth science research using terrestrial laser scanning. *Earth-Science Reviews*, *169*, 35–68. https://doi.org/10.1016/j.earscirev.2017.04.007

Torres, E., & Saraiva, O. F. (1999). *Camadas de impedimento mecânico do solo em sistemas agrícolas com a soja*. *Embrapa Soja, Circular Técnica*. Londrina.

Tsunetaka, H., Hotta, N., Hayakawa, Y. S., & Imaizumi, F. (2020). Spatial accuracy assessment of unmanned aerial vehicle-based structures from motion multi-view stereo photogrammetry for geomorphic observations in initiation zones of debris flows, Ohya landslide, Japan. *Progress in Earth and Planetary Science*, *7*(24), 1–14. https://doi.org/10.1186/s40645-020-00336-0

van den Eeckhaut, M., Poesen, J., Gullentops, F., Vandekerckhove, L., & Hervás, J. (2011). Regional mapping and characterisation of old landslides in hilly regions using LiDAR-based imagery in Southern Flanders. *Quaternary Research*, *75*(3), 721–733. https://doi.org/10.1016/j.yqres.2011.02.006

van den Eeckhaut, M., Poesen, J., Verstraeten, G., Vanacker, V., Nyssen, J., Moeyersons, J., et al. (2007). Use of LIDAR-derived images form mapping old landslides under forest. *Earth Surface Processes and Landforms*, *32*, 754–769. https://doi.org/10.1002/esp

Vosselman, G., & Maas, H.-G. (2010). *Airborne and Terrestrial Laser Scanning*. (G. Vosselman & H.-G. Maas, Eds.) *Current* (1st ed.). Dunbeath, Scotland, UK: Whittles Publishing. https://doi.org/10.1080/17538947.2011.553487

Xu, Q., Li, W., Ju, Y., Dong, X., & Peng, D. (2020). Multitemporal UAV-based photogrammetry for landslide detection and monitoring in a large area: a case study in the Heifangtai terrace in the Loess Plateau of China. *Journal of Mountain Science*, *14*, 1826–1839. https://doi.org/https://doi.org/10.1007/s11629-020-6064-9

Yeh, T. W., & Chuang, R. Y. (2020). Morphological analysis of landslides in extreme topography by UAS-SfM: data acquistion, 3D models and chenge detection. *The International Archives of the Photogrammetry, Remote Sensing and Spatial Information Sciences*, *XLIII-B5-2020*, 173–178. https://doi.org/10.5194/isprs-archives-XLIII-B5-2020-173-2020

Yu, M., Huang, Y., Zhou, J., & Mao, L. (2017). Modeling of landslide topography based on micro-unmanned aerial vehicle photography and structure-from-motion. *Environmental Earth Sciences*, *76*(520), 1–9. https://doi.org/10.1007/s12665-017-6860-x

Zhang, W., Qi, J., Wan, P., Wang, H., Xie, D., Wang, X., & Yan, G. (2016). An Easy-to-Use Airborne LiDAR Data Filtering Method Based on Cloth Simulation. *Remote Sensing*, *8*(6), 1–22. https://doi.org/https://doi.org/10.3390/rs8060501

# ADDITIONAL INFORMATION

## Data Availability

The point cloud datasets used in this study are available via the OpenTopography Facility (https://opentopography.org/). The following datasets were used: OpenTopography ID OTDS.082019.32723.1 (SfM-MVS), OTDS.082019.32723.2 (TLS).